Concentration and Speciation of Mercury in Atmospheric Particulates in the Wuda Coal Fire Area, Inner Mongolia, China

Yahui Qian
China University of Mining and Technology - Beijing Campus
Yanci Liang
Minzu University of China
Qingyi Cao
China University of Mining and Technology - Beijing Campus
Zhe Wang
China University of Mining and Technology - Beijing Campus
Yunyun Shi
China University of Mining and Technology - Beijing Campus
Handong Liang (hdl6688@cumtb.edu.cn)
China University of Mining and Technology

Research Article

Keywords: mercury, atmospheric particulate matter, atmospheric mercury, particulate mercury speciation, coal fire, Wuda

Posted Date: June 18th, 2021

DOI: https://doi.org/10.21203/rs.3.rs-573885/v1

Version of Record: A version of this preprint was published at Environmental Science and Pollution Research on August 16th, 2021. See the published version at https://doi.org/10.1007/s11356-021-15805-2.

Abstract

Coal-seam fire is a source of atmospheric mercury that is difficult to control. The Wuda Coalfield in Inner Mongolia, China, is one of the most severe coal fire disaster areas in the world and has been burning for more than 50 years. To investigate atmospheric mercury pollution from the Wuda coal fire, gaseous elemental mercury (GEM) concentrations and atmospheric particulate mercury (PHg) speciation were measured using a RA-915 + mercury analyzer and the temperature-programmed desorption (TPD) method. Near-surface GEM concentrations in the Wuda Coalfield and adjacent urban area were 80 ng m^{-3} (65–90 ng m^{-3}) and 52 ng m^{-3} (25–95 ng m^{-3}), respectively, which are far higher than the local background value (22 ng m^{-3}). PHg concentrations in the coalfield and urban area also reached significantly high levels, at 33 ng m^{-3} (25–45 ng m^{-3}) and 22 ng m^{-3} (14–29 ng m^{-3}), respectively. There is no clear evidence that PHg combines with organic carbon (OC) or elemental carbon (EC), but PHg concentration appears to be controlled by air acidity. PHg mainly exists in inorganic forms, such as $HgCl_2$, HgS, HgO, and $Hg(NO_3)_2{\cdot}H_2O$. This work can provide references for the speciation analysis of atmospheric PHg and the safety assessment of environmental mercury.

Introduction

Coal fires are a global catastrophe and have been reported in many countries and regions, such as the United States, Australia, South Africa, India, and China (Heffern and Coates, 2004; Kuenzer and Stracher, 2012; Mishra et al., 2011; Pone et al., 2007; Sharygin et al., 2009; Zhang et al., 2004). Heat generated by the oxidation of sulfides accumulates in the coal seam, and fires occur as the heat continues to increase (Heffern and Coates, 2004; Walker, 1999). Coal fires consume large amounts of coal resources and cause ground collapse (Kuenzer and Stracher, 2012); they also release large concentrations of toxic and harmful gases to the atmosphere, including Hg, CO, SOx, NOx, and volatile organic compounds (VOCs) (Finkelman, 2004; Hower et al., 2011; O'Keefe et al., 2011). The Wuda Coalfield, Inner Mongolia, is one of 14 large-scale coal bases in China, and it is also one of the most severe coal fire disaster areas in the world (Liang et al., 2014). Underground coal fires in this area have been burning for more than 50 years (Zhang et al., 2008), and the annual coal loss is approximately 20×10^7 t, which exceeds the annual coal output of Germany (Cao et al., 2018). Local soil, dust fall, and air mercury pollution caused by coal fires have therefore attracted significant attention from the research community (Liang et al., 2014; Liang et al., 2016; Liang et al., 2018; Li et al., 2018). Unfortunately, no effective measures are in place to curb coal fire pollution.

Mercury is a heavy metal pollutant with high neurotoxicity and a strong affinity for bioaccumulation (Fu et al., 2011). It is prone to long-range transportation and can be found in remote areas away from emission sources (Chance et al., 2015; Soriano et al., 2012). Atmospheric mercury can enter surface soil and water via dry–wet deposition (Ariya et al., 2004; Harada, 2005). It can also return to the atmosphere via evasion fluxes from the water-air and soil-air interfaces, thus forming the global mercury cycle (Kalinchuk et al., 2021; Bowman et al., 2019; Ci et al., 2011; Windham-Myers et al., 2013; Yang et al., 2020). Generally, gaseous elemental mercury (GEM) is the primary form of atmospheric mercury, and atmospheric particulate mercury (PHg) often contributes less than 10% to the total atmospheric mercury (Feng et al., 2013; Fu et al., 2010; Miller et al., 2021). However, GEM is known to convert to PHg under certain oxidative conditions (Ebinghaus et al., 2002; Obrist et al., 2011; Weiss-Penzias et al., 2015). The regional sedimentation and water solubility of PHg are stronger than that of GEM (Sun et al., 2020), and it can enter and permanently damage the human body through inhalation, dietary consumption, and skin exposure (Trasande et al., 2005).

Current studies have had variable levels of success in measuring the atmospheric mercury concentration globally (Landis et al., 2002; Cheng and Zhang, 2017; Zhang et al., 2017; Fu et al., 2010). However, the chemical form of atmospheric PHg has been studied only rarely. This is because the concentration of PHg in ordinary environments is

often < 2 ng/m^3, making it difficult to enrich; there is also a lack of effective analysis methods. The Wuda coalfield, a typical PHg enrichment area, provides favorable conditions for analyzing the speciation of PHg. This study examined the concentration and speciation of PHg in the Wuda Coalfield fire area using a variety of experimental data. The results can provide references for the speciation analysis of atmospheric PHg and the safety assessment of environmental mercury.

Materials And Methods

2.1. Study area

The Wuda District of Wuhai City (39°20'–39°40' N, 106°30'–106°50' E) is located in central Inner Mongolia in northern China; it is situated at the southern edge of the Ulan Buh Desert, the northern end of Helan Mountain, and the eastern border of the Yellow River. The district is in a temperate zone, with an annual average wind speed of 4.8 m s^{-1} (northwesterly winds prevail in the local area), average annual rainfall of 176.9 mm, and average annual evaporation of 3,641 mm. The Wuda Coalfield is located in the northwest of the Wuda District and has an area of 35 km^2. It is rich in Carboniferous-Permian coal, with a reserve of 660 million tons, and mainly produces bituminous coal. The Wuda urban area is located approximately 6 km southeast of the coalfield and is one of the economic development zones approved by Inner Mongolia in 1998. The coal-seam fire in the Wuda Coalfield began in 1961 and was caused by the non-standard mining of small coal kilns (Liang et al., 2014). Six fire zones had formed in the surface mining area by 1978, which increased to 26 in 2004, covering a total area of ~ 4 km^2. Numerous attempts have been made to control the localized coal fire since 2009, but the coal fire trends remain volatile and uncontrollable.

2.2. Sample collection

The atmospheric PHg samples were collected in coal fire areas (located in the northwest) and neighboring urban areas (located in the southeast) in August and September 2015. In the coal fire area, on-site collection and testing activities avoided the underground flue gas discharge channel to ensure this investigation was objective and representative. An MLY-60 atmospheric particulate sampler was used to collect the total suspended particles (TSP) and $PM_{2.5}$ samples. The collection flow of the sampler was 20 L min^{-1}, and the collection height was 1.5 m above the ground. The atmospheric particle sampling membrane was a quartz filter membrane with a diameter of 47 mm. The quartz filter membrane was baked in a muffle furnace at 550°C for 6 h before use. After natural cooling, it was placed in an equilibrium chamber at a relative humidity of 35% and a temperature of 22°C for 24 h. The filter membrane was then weighed with a precision of 0.0001 g using an electronic balance and loaded into the membrane box. Mercury was not detected in the treated quartz filtration membrane. The collected samples were rebalanced and weighed in a balance room under constant temperature and humidity before being placed in cold storage. A total of 12 samples from the coalfield fire areas and 23 samples from the urban area were collected.

2.3. Experimental

2.3.1. OC/EC testing

A DRI Model 2001 carbon analyzer (American Desert Research Institute) was used to determine the organic carbon (OC) and elemental carbon (EC) content of the atmospheric particulate samples. At present, thermal decomposition optical analysis is a recognized and mature method for the determination of OC and EC contents. Depending on the optical correction methods, the process can be divided into thermal–optical reflection (TOR) and thermal–optical transmission (TOT). The measurement principles of the two methods are similar, but the obtained results are different due to the time difference of the laser segmentation point (Shen et al., 2011). The DRI Model 2001 can provide both TOR and TOT data

based on the thermal–optical analysis principle, resulting in more comprehensive data analysis. The analysis area was 0.552 cm^2, intercepted by a circular punch. The test results were converted to air concentrations according to the sampling volume.

2.3.2. Water-soluble ion and pH testing

For the atmospheric particulate samples, 10 inorganic water-soluble ions (F^-, Cl^-, NO_3^-, NO_2^-, SO_4^{2-}, Na^+, NH_4^+, K^+, Ca^{2+}, and Mg^{2+}) were determined using an IC-8610 ion chromatograph (Qingdao Luhai Optoelectronics Technology Co., Ltd.). A quarter of the sample membrane was placed in a beaker, 10 mL of deionized water was added, and the mixture was then sonicated for 30 min. After standing for 60 min, the supernatant was collected for the experimental test. The anion test was performed using an IonPac AS19 separation column. The injection volume was 25 µL, and the eluent was a 25 mmol L^{-1} NaOH solution with a flow rate of 1.2 mL min^{-1}. The cations were separated using an IonPac CS12 column. The eluent was 30 mmol L^{-1} MSA solution with a flow rate of 1 mL min^{-1} and an injection volume of 25 µL. The linear fitting degree of the anion and cation standard curves was better than 0.999, and the detection limit (S/N = 3) was less than 0.02 mg L^{-1}. Three blank experiments were also performed, and their experimental mean value was used as the background value. The equivalent concentration obtained by the test was converted to air concentration. In addition, a pH meter (Mettler Toledo) was used to measure the acidity of the aqueous solution after sonication. Before measurement, the instrument was calibrated with a pH standard solution (pH = 4.01, 7.00, 9.02).

2.3.3. Mercury concentration testing

The GEM concentration in the air was measured using an RA-915 + mercury analyzer (Lumex Ltd., Russia), which employs Zeeman atomic absorption spectrometry with a high frequency modulation of light polarization. The gas detection limit of the instrument was 2 ng m^{-3}, and the signal response time frequency was 1 s^{-1}, making it suitable for real-time measurements of GEM (Hong et al., 2017; Li et al., 2018; Liang et al., 2014). The mercury content of the particulate matter samples was measured using the RA-915 + combined with a Pyro-915 + pyrolysis device, and 1/4 of the sample area was used. The standard curve was calibrated using GBW07447 (GSS-18) standard Hg soil (15 ng g^{-1}), with a linear correlation coefficient (R) of 0.999.

2.3.4. Temperature-programmed desorption (TPD)

TPD combined with atomic absorption spectrometry (AAS) technology is suitable for the comprehensive analysis of Hg species in solid samples (Cao et al., 2020a; Cao et al., 2020b). The TPD experimental system was predominately composed of an argon gas supply device, an SK-G04123K tube pyrolysis furnace, an RA-915 + mercury analyzer, and an exhaust gas adsorption device (Fig. 1). The heating range was 25–650°C at a heating rate of 10°C min^{-1}, and the argon purge rate was 1.0 L min^{-1}.

Results

3.1 Atmospheric Hg concentration

The wind direction was northwesterly during the entire sampling period, which is consistent with the perennial wind direction of the region, with a wind speed range of 0.6–5.2 m s^{-1}. To evaluate the level of atmospheric mercury pollution in the Wuda region, the GEM content at the coal field boundary northwest of the Wuda District was measured for use as the background value. The data were recorded every 5 s, and the real-time measurement lasted 3 min. According to the on-site monitoring data, the background GEM concentration ranged from 13 to 29 ng m^{-3}, with an average value of 22 ng m^{-3}, which far exceeds the global atmospheric mercury background value (1.5–1.8 ng m^{-3})

(Jaffe et al., 2005). The average GEM concentrations in the Wuda Coalfield and the adjacent urban area were 80 ng m^{-3} (65–90 ng m^{-3}) and 52 ng m^{-3} (25–95 ng m^{-3}), respectively, which was 3.6 and 2.4 times the background level of the area, respectively. The concentrations were far higher than those in other typical industrial cities or regions, such as Guiyang (9.72 ng m^{-3}) (Fu et al., 2011), Guangzhou (5.4 ng m^{-3}) (Wang et al., 2007), Changchun (18.4 ng m^{-3}) (Fang et al., 2001), and Taiwan (6.3–9.4 ng m^{-3}) (Kuo et al., 2006).

The Hg content of TSP in the Wuda Coalfield and adjacent urban area were 25–45 ng m^{-3} and 14–29 ng m^{-3}, with average contents of 33 ng m^{-3} and 21 ng m^{-3}, respectively. The average PHg concentration in the TSP samples from the Wuda Coalfield was 28, 77, and 33 times that of Beijing (1.18 ng m^{-3}) (Liu et al., 2002), Shanghai (0.429 ng m^{-3}) (Xiu et al., 2003), and Changchun (0.022–1.98 ng m^{-3}) (Fang et al., 2001), respectively, indicating significant localized atmospheric mercury pollution caused by coalfield fires.

Using a scanning electron microscope (SEM-EDX) to analyze the morphology and chemical composition of 1,600 single atmospheric particles in the Wuda urban area, Wang et al. (2018) found that mineral particles, combustion particles, and sulfur-containing particles were the main particle forms in the region, which contained abundant weathered coal gangue and raw coal dust particles. This suggests that the atmospheric pollutants from the coal field fires were transmitted to the downwind urban area. It should be noted that this study omitted the contribution of other potential mercury pollution sources (such as transportation, biomass combustion, industrial waste gas, and other long-distance transportation of particulate matter). The Wuda area has significant atmospheric mercury concentrations, despite its much lower population size and total gross domestic product (GDP) than those of the other cities listed in this manuscript. This suggests that the coal fires are the highest mercury contributors in the area, with other source factors contributing significantly less in comparison.

3.2 Correlation between PHg content and OC/EC content in TSP

OC and EC are mainly derived from coal combustion, motor vehicle emissions, and biomass combustion. Moreover, EC is more stable and is principally sourced from the primary combustion emissions of coal (Gray et al., 1986; Salma et al., 2004; Viana et al., 2006). The total carbon (TC) concentration in TSP in the Wuda urban area during the sampling period varied from 59.57 to 134.49 μg m^{-3}, with an average value of 87.73 μg m^{-3}. The OC and EC contents measured by the TOT method were 48.88 μg m^{-3} (30.08–64.95 μg m^{-3}) and 41.95 μg m^{-3} (29.50–69.54 μg m^{-3}), respectively. Using the TOR method, the OC and EC contents were 57.25 μg m^{-3} (29.2–96.56 μg m^{-3}) and 30.58 μg m^{-3} (17.53–48.05 μg m^{-3}), respectively. The TC content of TSP in the Wuda urban area was 1.9 and 4.4 times that of the typical Chinese industrial cities of Tangshan (47 μg m^{-3}, 30–64 μg m^{-3}) (Guo et al., 2013) and Harbin (19.81 μg m^{-3}, 9.35–35.12 μg m^{-3}) (Huang, 2013), respectively.

We observed no correlation between PHg content and OC/EC content in TSP. The correlation coefficients (r) did not exceed 0.1 in the TOR and TOT modes (Fig. 2). This suggests that mercury in atmospheric particles is less likely to exist in its organic state and is also unlikely to be adsorbed on the surface of carbon particles in its elemental state. Therefore, mercury in atmospheric particles is more likely to occur in the form of inorganic compounds.

3.3 Correlation between PHg content and water-soluble ion content in TSP and $PM_{2.5}$

Water-soluble ions are an important component of atmospheric particles (Behrooz et al., 2017a; Chakraborty and Gupta, 2010). They are mostly composed of cations such as NH_4^+, K^+, Ca^{2+}, Na^+, and Mg^{2+}, and anions such as SO_4^{2-}, NO_3^-, Cl^-, and F^-. In coastal cities, SO_4^{2-}, NO_3^-, Cl^-, and Na^+ are largely derived from sea salt particles, whereas in inland cities they are largely derived from fossil fuel combustion, the chlor-alkali industry, and other production activities.

Moreover, K^+ is mostly derived from biomass combustion (Alastuey et al., 2006; Behrooz et al., 2017b; Bisht et al., 2015; Zhang et al., 2013). The content ranges of F^-, Cl^-, NO_2^-, NO_3^-, and SO_4^{2-} in TSP in the Wuda urban area were 0.08–1.41, 15.48–32.94, 0.09–0.38, 6.73–12.38, and 17.85–40.7 μg m^{-3}, respectively, and their average values were 0.83, 22.75, 0.24, 9.50, and 25.15 μg m^{-3}, respectively. In $PM_{2.5}$, the same ions yielded contents of 0.09 μg m^{-3} (0.02–0.21 μg m^{-3}), 10.69 μg m^{-3} (6.43–18.56 μg m^{-3}), 0.13 μg m^{-3} (0.02–0.26 μg m^{-3}), 8.71 μg m^{-3} (5.93–11.90 μg m^{-3}), and 10.291 μg m^{-3} (7.11–15.01 μg m^{-3}), respectively, accounting for 10, 47, 56, 92, and 41% of the corresponding ion concentrations in TSP, respectively. Moreover, SO_4^{2-}, Cl^-, and NO_3^- were the dominant anions, accounting for approximately 43, 39, and 16% of the total anion concentration, respectively.

Based on Pearson's correlation analysis, the PHg content was significantly correlated with Cl^- and NO_3^- in $PM_{2.5}$, and the corresponding r values were 0.854 and 0.745, respectively (Table 1). This indicates that Hg tends to combine with Cl^- and NO_3^- to form mercury particles, likely as $HgCl_2$ and $Hg(NO_3)_2$. We also observed a high correlation between PHg and NO_3^- in TSP (r = 0.643). The Cl^- in TSP showed no clear correlation with PHg, but was closely related to Na^+ (r = 0.890) (Table 2). This suggests that the association between Cl^- and PHg in TSP may be masked by the interference of NaCl particles. In addition, PHg was correlated with Ca^+, Na^+, and Mg^{2+} contents in $PM_{2.5}$ (Table 1). However, this may be an indirect effect caused by the correlation between Ca^+, Na^+, Mg^{2+}, and NO_3^-/Cl^- (Table 1). The contents of Cl^- and NO_3^- in $PM_{2.5}$ accounted for 47 and 92% of the corresponding ion concentrations in TSP, respectively, indicating that PHg predominantly occurs as fine particulate matter.

Some studies have shown that burning coal produces SO_2 and NO_2, which subsequently forms H_2SO_4 and HNO_3 through oxidation and moisture absorption (Fang and Liu, 2010; Pathak et al., 2009; Tatu et al., 2006). As shown in Fig. 3, the TSP sampling volume from the coalfield fire area ranged from 11,476 to 25,490 L (average 17,849 L), with corresponding solution pHs of 3.28–4.81; the TSP sampling volume from the urban area was 43,859–45,533 L (average 44,515 L), with corresponding solution pHs of 5.43–6.41. The sampling volumes from the coalfield fire area were smaller but produced more acid; this suggests that the acidic gas produced by the combustion of underground coal fires was the main source of acid in this area and may also be transported to other areas through airflow migration. We observed a significant negative correlation between PHg content and acidity in TSP (r = -0.906), as PHg more easily accumulates in acidic environments.

3.4 Analysis of PHg speciation based on AAS-TPD

Figure 4 shows the thermal decomposition curves of Hg in the TSP samples collected from the Wuda mining and urban areas under an argon atmosphere. Mercury decomposition predominantly occurs in the range of 150–450°C. Owing to the coexistence of various mercury species with different thermal stability characteristics, multiple Hg signal peaks appear in this temperature range (Cao et al., 2019a; Cao et al., 2019b). To clear the individual mercury peak ranges, Origin 6.0 software was used to deconvolve the mercury decomposition curves and obtain four peaks (A, B, C, and D) (Fig. 4). The starting temperature ranges of the four TSP peaks from the coalfield area were 173–253, 276–335, 320–380, and 367–379°C, with the center peaks at 213, 306, 350, and 373°C, respectively. The corresponding TSP ranges from the urban area were 185–268, 275–335, 265–412, and 367–389°C, with the central peaks at 223, 305, 340, and 378°C, respectively. The thermal decomposition characteristics of PHg in the two regions were consistent, indicating the same species of Hg.

Compared with the thermal decomposition characteristics of standard mercury compounds (Table 3), the characteristic peaks of $HgCl_2$, HgS, HgO, and $Hg(NO_3)_2 \cdot H_2O$ occurred near 212, 310, 340, and 373°C, respectively (Liu et al., 2013; Lopez-Anton et al., 2011; Lv, 2017; Meng and Wang, 2012; Wang, 2016). The starting ranges of the characteristic peaks

are highly consistent with peaks A, B, C, and D. The mercury in atmospheric particles in the study area therefore likely exists mainly in the forms of $HgCl_2$, HgS, HgO, and $Hg(NO_3)_2{\cdot}H_2O$. This is consistent with the high correlation between PHg, Cl^-, and NO_3^- obtained by water-soluble ion analysis.

Based on the deconvolution results, the contents of $HgCl_2$, HgS, HgO, and $Hg(NO_3)_2{\cdot}H_2O$ in atmospheric particles from the coalfield area accounted for 9, 23, 58, and 10%, respectively. The proportions in the urban area were similar, with corresponding rates of 15%, 30%, 41%, and 14%.

Conclusion

The near-surface GEM and PHg concentrations in the Wuda Coalfield, Inner Mongolia, China were 80 ng m^{-3} (65–90 ng m^{-3}) and 33 ng m^{-3} (25–45 ng m^{-3}). Under the influence of coal fires, the GEM and PHg concentrations in the downwind urban area reached 33 ng m^{-3} (25–45 ng m^{-3}) and 22 ng m^{-3} (14–29 ng m^{-3}), respectively. The PHg content was found to be related to NO_3^- and Cl^- in atmospheric particles, and this was manifested more strongly in $PM_{2.5}$. The PHg concentration in atmospheric particulates is closely related to acidity (r = -0.906). Our results suggest that PHg in the atmosphere may predominantly exist as inorganic forms, such as $HgCl_2$, HgS, HgO, and $Hg(NO_3)_2{\cdot}H_2O$, and also tends to occur in the form of fine particles (≤ 2.5 μm). This work can thus act as a reference for analyzing the speciation of atmospheric PHg and the safety assessment of environmental mercury.

Declarations

Acknowledgements

We appreciate the comments and suggestions from anonymous reviewers who can greatly improve this paper.

Availability of data and materials

The datasets used or analyzed during the current study are available from the corresponding author on reasonable request.

Author contribution

Yahui Qian: Experiments, Sample analyses, Data interpretation and presentation, Writing original draft; Yanci Liang: Conceptualization, review and editing; Qingyi Cao: Data analysis, interpretation and editing; Zhe Wang and Yunyun Shi: Sample collection and Experiments; Handong Liang: Conceptualization, Supervision, Validation, Review and editing. All authors read and approved the final manuscript.

Funding

This study was financially supported by a project supported by the National Natural Science Foundation of China (41371449), and the State Key Laboratory of Coal Resources and Safe Mining (SKLCRSM19ZZ03).

Ethics approval and consent to participate Not applicable.

Consent for publication Written informed consent for publication was obtained from all participants.

Competing interests The authors declare no competing interests.

References

1. Alastuey, A., Querol, X., Plana, F., Viana, M., Ruiz, C.R., de la Campa, A.S., de la Rosa, J., Mantilla, E., dos Santos, S.G., 2006. Identification and chemical characterization of industrial particulate matter sources in southwest Spain. Journal of the Air & Waste Management Association 56, 993-1006. https://dio.org/10.1080/10473289.2006.10464502
2. Ariya, P.A., Ryzhkov, A., Davignon, D., Lalonde, J., Steffen, A., 2004. The Arctic: a sink for mercury. Tellus Series B-Chemical and Physical Meteorology 56, 397-403. https://dio.org/10.1111/j.1600-0889.2004.00118.x
3. Behrooz, R.D., Esmaili-Sari, A., Bahramifar, N., Kaskaoutis, D.G., 2017a. Analysis of the TSP, PM10 concentrations and water-soluble ionic species in airborne samples over Sistan, Iran during the summer dusty period. Atmos. Pollut. Res. 8, 403-417. https://dio.org/10.1016/j.apr.2016.11.001
4. Behrooz, R.D., Esmaili-Sari, A., Bahramifar, N., Kaskaoutis, D.G., Saeb, K., Rajaei, F., 2017b. Trace-element concentrations and water-soluble ions in size-segregated dust-borne and soil samples in Sistan, southeast Iran. Aeolian Research 25, 87-105. https://dio.org/10.1016/j.aeolia.2017.04.001
5. Bisht, D.S., Dumka, U.C., Kaskaoutis, D.G., Pipal, A.S., Srivastava, A.K., Soni, V.K., Attri, S.D., Sateesh, M., Tiwari, S., 2015. Carbonaceous aerosols and pollutants over Delhi urban environment: Temporal evolution, source apportionment and radiative forcing. Sci. Total Environ. 521, 431-445. https://dio.org/10.1016/j.scitotenv.2015.03.083
6. Bowman, K.L., Lamborg, C.H., Agather, A.M., 2019. A global perspective on mercury cycling in the ocean. Sci. Total Environ. 136166. https://doi.org/10.1016/j.scitotenv.2019.136166
7. Cao, Q.Y., Liang, H.D., Chen, Y., Li, Z.W., Liu, H.W., 2018. Distribution of mercury content in topsoil of coal base, Wuda, China. J. Min. Sci. 3: 315-322. DOI: 10.19606/j.cnki.jmst.2018. 04.001
8. Cao, Q.Y., Liang, H.D., Li, C.H., Yang, L., 2019a. Analysis of mercury speciations in Late Permian coal from the border area of Yunnan, Guizhou and Sichuan provinces. China Environmental Science 39, 3959-3966. https://dio.org/10.19674/j.cnki.issn1000-6923.2019.0464
9. Cao, Q.Y., Qian, Y.H., Liang, H.D., Wang, Z., 2019b. The species and spatial distribution characteristics of atmospheric particulate mercury in Wuda-Wusitai Industrial Park, China. China Environmental Science 39(12):4989-4998. DOI: 10.19674/j.cnki.issn1000-6923.2019.0580
10. Cao, Q.Y., Qian, Y.H., Liang, H.D., Li, Z.W., Chen, S.Y., Yang, L., Zhan, Q., 2020a. Mercury forms and their transformation in pyrite under weathering. Surf. Interface Anal. 52 (2), 283–292. https://doi.org/10.1002/sia.6718.
11. Cao QY, Yang L, Qian YH, Liang, HD. Study on Mercury Species in Coal and Pyrolysis-Based Mercury Removal before Utilization. ACS Omega. 2020b,5(32): 20215-20223. DOI: 10.1021/acsomega.0c01875
12. Chakraborty, A., Gupta, T., 2010. Chemical Characterization and Source Apportionment of Submicron (PM1) Aerosol in Kanpur Region, India. Aerosol and Air Quality Research 10, 433-445. https://dio.org/10.4209/aaqr.2009.11.0071
13. Chance, R., Jickells, T.D., Baker, A.R., 2015. Atmospheric trace metal concentrations, solubility and deposition fluxes in remote marine air over the south-east Atlantic. Mar. Chem. 177, 45–56. https://dio.org/10.1016/j.marchem.2015.06.028
14. Cheng, I., Zhang, L., 2017. Uncertainty assessment of gaseous oxidized mercury measurements collected by atmospheric mercury network. Environ. Sci. Technol. 51, 855-862. https://doi.org/10.1021/acs.est.6b04926
15. Ci, Z. J., Zhang, X. S., Wang, Z. W., Niu, Z. C., Diao, X. Y., Wang, S. W., 2011. Distribution and air-sea exchange of mercury (Hg) in the Yellow Sea. Atmos. Chem. Phys., 11(6): 2881–2892. doi:10.5194/acp-11-2881-2011
16. Ebinghaus, R., Kock, H.H., Temme, C., Einax, J.W., Löwe, A.G., Richter, A., et al., 2002. Antarctic springtime depletion of atmospheric mercury. Environ. Sci. Technol. 36, 1238–1244. https://doi.org/10.1021/es015710z

17. Fang, F., Wang, Q., Li, J., 2001. Atmospheric particulate mercury concentration and its dry deposition flux in Changchun City, China. Sci. Total Environ. 281: 229–236. doi:10.1016/s0048-9697(01)00849-x
18. Fang, G.C., Liu, C.K., 2010. Ambient suspended particulate matter and ionic speciation in Asian countries during 1998-2007. Toxicol. Ind. Health26, 589-600. https://dio.org/10.1177/0748233710375950
19. Feng, X.B., Chen, J.B., Fu, X.W., Hu, H.Y., Li, P., Chou, G.L., Yan, H.Y., Yin, R.S., Zhang, H., Zhu, W., 2013. Progresses on environmental geochemistry of mercury. Bulletin of Mineralogy, Petrology and Geochemistry 32, 503-530. (in Chinese)
20. Finkelman, R.B., 2004. Potential health impacts of burning coal beds and waste banks. Int. J. Coal Geol. 59, 19-24. https://dio.org/10.1016/j.coal.2003.11.002
21. Fu, X.W., Feng, X., Dong, Z.Q., Yin, R.S., Wang, J.X., Yang, Z.R., Zhang, H., 2010. Atmospheric gaseous elemental mercury (GEM) concentrations and mercury depositions at a high-altitude mountain peak in south China. Atmos. Chem. Phys. 10, 2425-2437. https://dio.org/10.5194/acp-10-2425-2010
22. Fu, X.W., Feng, X.B., Sommar, J., Wang, S.F., 2011. A review of studies on atmospheric mercury in China. Sci. Total Environ. 421, 73-81. https://dio.org/10.1016/j.scitotenv.2011.09.089
23. Gray, H.A., Cass, G.R., Huntzicker, J.J., Heyerdahl, E.K., Rau, J.A., 1986. Characteristics of atmospheric organic and elemental carbon particle concentrations in Los Angeles. Environ. Sci. Technol. 20, 580-589. https://dio.org/10.1021/es00148a006.
24. Guo, Y.H., Xin, J.Y., Wang, Y.S., Wen, T.X., Li, X.R., Feng, X.X., 2013. Observation and study of OC/EC concentration spectrum distribution of atmospheric particles in tangshan city. Environmental science 34: 2497-2504. DOI: 10.13227/j.hjkx.2013.07.020
25. Harada, M., 2005. The global lessons of Minamata disease: an introduction to Minamata studies. Emerald Group Publishing Limited, Scotland.
26. Heffern, E.L., Coates, D.A., 2004. Geologic history of natural coal-bed fires, Powder River basin, USA. Int. J. Coal Geol. 59, 25-47. https://dio.org/10.1016/j.coal.2003.07.002
27. Hower, J.C., O'Keefe, J.M.K., Henke, K.R., Baghereih, A., 2011. Time series analysis of CO concentrations from an Eastern Kentucky coal fire. Int. J. Coal Geol. 88, 227-231. https://dio.org/10.1016/j.coal.2011.10.001
28. Hong, X., Liang, H., Lv, S., Jia, Y., Zhao, T., & Liang, W., 2017. Mercury emissions from dynamic monitoring holes of underground coal fires in the Wuda Coalfield, Inner Mongolia, China. Int. J. Coal Geol., 181, 78–86. doi:10.1016/j.coal.2017.08.013
29. Huang, L.K., 2013. Study on OC and EC Characteristics of Atmospheric Particulate Matter in Harbin. Advanced Materials Research 777, 412–415. doi:10.4028/www.scientific.net/amr.777.412
30. Jaffe, D., Prestbo, E., Swartzendruber, P., Weiss-Penzias, P., Kato, S., Takami, A., Hatakeyama, S., Kajii, Y., 2005. Export of atmospheric mercury from Asia. Atmos. Environ. 39, 3029-3038. https://dio.org/10.1016/j.atmosenv.2005.01.030
31. Kuo, T.H., Chang, C.F., Urba, A., Kvietkus, K., 2006. Atmospheric gaseous mercury in Northern Taiwan. Sci. Total Environ. 368(1), 10–18. doi:10.1016/j.scitotenv.2005.10.017
32. Kuenzer, C., Stracher, G.B., 2012. Geomorphology of coal seam fires. Geomorphology 138, 209-222. https://dio.org/10.1016/j.geomorph.2011.09.004
33. Kalinchuk, Viktor V.; Lopatnikov, Evgeny A.; Astakhov, Anatoliy S.; Ivanov, Maxim V.; Hu, Limin (2021). Distribution of atmospheric gaseous elemental mercury (Hg(0)) from the Sea of Japan to the Arctic, and Hg(0) evasion fluxes in the Eastern Arctic Seas: Results from a joint Russian-Chinese cruise in fall 2018. Sci. Total Environ. 753, 142003. doi:10.1016/j.scitotenv.2020.142003

34. Landis, M.S., Stevens, R.K., Schaedlich, F., Prestbo, E.M., 2002. Development and characterization of an annular denuder methodology for the measurement of divalent inorganic reactive gaseous mercury in ambient air. Environ. Sci. Technol. 36, 3000-3009. https://doi.org/10.1021/es015887t
35. Li, C.H., Liang, H.D., Chen, Y., Bai, J.W., Cui, Y.K., 2018. Distribution of surface soil mercury of Wuda old mining area, Inner Mongolia, China. Human and Ecological Risk Assessment 24, 1421-1439. https://dio.org/10.1080/10807039.2017.1413536
36. Liang, Y.C., Liang, H.D., Zhu, S.Q., 2014. Mercury emission from coal seam fire at Wuda, Inner Mongolia, China. Atmos. Environ. 83, 176-184. https://dio.org/10.1016/j.atmosenv.2013.09.001
37. Liang, Y.C., Zhu, S.Q., Liang, H.D., 2016. Mercury emission from spontaneously ignited coal gangue hill in Wuda coalfield, Inner Mongolia, China. Fuel, 182, 525-530. https://doi.org/10.1016/j.fuel.2016.05.092
38. Liang, Y.C., Zhu, S.Q., Liang, H.D., 2018. Mercury enrichment in coal fire sponge in Wuda coalfield, Inner Mongolia of China. Int. J. Coal Geol. 192, 51-55. https://dio.org/10.1016/j.coal.2018.03.006
39. Liu, X.L., Wang, S.X., Zhang, L., Wu, Y., Duan, L., Hao, J.M., 2013. Speciation of mercury in FGD gypsum and mercury emission during the wallboard production in China. Fuel 111, 621-627. https://dio.org/10.1016/j.fuel.2013.03.052
40. Liu, S., Nadim, F., Perkins, C., Carley, R. J., Hoag, G. E., Lin, Y., Chen, L., 2002. Atmospheric mercury monitoring survey in Beijing, China. Chemosphere, 48(1), 97-107. doi:10.1016/s0045-6535(02)00026-7
41. Lopez-Anton, M.A., Perry, R., Abad-Valle, P., Diaz-Somoano, M., Martinez-Tarazona, M.R., Maroto-Valer, M.M., 2011. Speciation of mercury in fly ashes by temperature programmed decomposition. Fuel Process. Technol. 92, 707-711. https://dio.org/10.1016/j.fuproc.2010.12.002
42. Lv, J., 2017. Research on mercury release behavior and speciation identification of coals, North China Electric Power University (Beijing). North China Electric Power University (Beijing), Beijing. (in Chinese)
43. Meng, Y., Wang, S.X., 2012. Study on mercury re-emissions during fly ash utilization. Environment Science 33, 2993-2999. DOI: 10.13227/j.hjkx.2012.09.036
44. Miller, M. B., Howard, D. A., Pierce, A. M., Cook, K. R., Keywood, M., Powell, J., Gustin, M. S., Edwards, G. C. (2021). Atmospheric reactive mercury concentrations in coastal Australia and the Southern Ocean. Sci. Total Environ. 751, 141681. doi:10.1016/j.scitotenv.2020.141681
45. Mishra, R.K., Bahuguna, P.P., Singh, V.K., 2011. Detection of coal mine fire in Jharia Coal Field using Landsat-7 ETM+ data. Int. J. Coal Geol. 86, 73-78. https://dio.org/10.1016/j.coal.2010.12.010
46. Obrist, D., Tas, E., Peleg, M., Matveev, V., Fain, X., Asaf, D., et al., 2011. Bromine-induced oxidation of mercury in the mid-latitude atmosphere. Nat. Geosci. 4, 22-26. DOI: 10.1038/NGEO1018
47. O'Keefe, J.M.K., Neace, E.R., Lemley, E.W., Hower, J.C., Henke, K.R., Copley, G., Hatch, R.S., Satterwhite, A.B., Blake, D.R., 2011. Old smokey coal fire□Floyd County□Kentucky: estimates of gaseous emission rates. Int. J. Coal Geol. 87, 150-156. https://dio.org/10.1016/j.coal.2011.06.005
48. Pathak, R.K., Wu, W.S., Wang, T., 2009. Summertime PM2.5 ionic species in four major cities of China: nitrate formation in an ammonia-deficient atmosphere. Atmos. Chem. Phys. 9, 1711-1722. https://dio.org/10.5194/acp-9-1711-2009
49. Pone, J.D.N., Hein, K.A.A., Stracher, G.B., Annegarn, H.J., Finkleman, R.B., Blake, D.R., McCormack, J.K., Schroeder, P., 2007. The spontaneous combustion of coal and its by-products in the Witbank and Sasolburg coalfields of South Africa. Int. J. Coal Geol. 72, 124-140. https://dio.org/10.1016/j.coal.2007.01.001
50. Salma, I., Chi, X.G., Maenhaut, W., 2004. Elemental and organic carbon in urban canyon and background environments in Budapest, Hungary. Atmos. Environ. 38, 27-36. https://dio.org/10.1016/j.atmosenv.2003.09.047

51. Sharygin, V.V., Sokol, E.V., Belakovskii, D.I., 2009. Fayalite-sekaninaite paralava from the Ravat coal fire (central Tajikistan). Russian Geology and Geophysics 50, 703-721. https://dio.org/10.1016/j.rgg.2009.01.001
52. Shen, Y., Liu, J.G., Lu, F., Ding, Q., Shi, J.G., 2011. Comparison of thermal-optical transmission and thermal-optical reflectance methods of measurement of organic and elemental carbon in atmospheric aerosol. Journal of Atmospheric and Environmental Optics 6, 450-456. https://dio.org/10.3969/j.issn.1673-6141.2011.06.008
53. Soriano, A., Pallarés, S., Pardo, F., Vicente, A.B., Sanfeliu, T., Bech, J., 2012. Deposition of heavy metals from particulate settleable matter in soils of an industrialised area. J. Geochem. Explor. 113, 36-44. https://doi.org/10.1016/j.gexplo.2011.03.006
54. Sun, G., Feng, X., Yang, C., Zhang, L., Yin, R., Li, Z., Bi, X., Wu, Y., 2020. Levels, sources, isotope signatures, and health risks of mercury in street dust across China. J. Hazard. Mater., 122276. https://doi.org/10.1016/j.jhazmat.2020.122276
55. Tatu, A., Astrid, K.-S., Ralf, T., F, M.T., 2006. On the reactive uptake of gaseous compounds by organic-coated aqueous aerosols: theoretical analysis and application to the heterogeneous hydrolysis of N_2O_5. The journal of physical chemistry Part A 110, 10435-10443. DOI:10.1021/jp062403c
56. Trasande, L., Landrigan, P.J., Schechter, C., 2005. Public health and economic consequences of methyl mercury toxicity to the developing brain. Environ. Health Perspect. 113, 590-596. https://dio.org/10.1289/ehp.7743
57. Viana, M., Chi, X., Maenhaut, W., Querol, X., Alastuey, A., Mikuska, P., Vecera, Z., 2006. Organic and elemental carbon concentrations in carbonaceous aerosols during summer and winter sampling campaigns in Barcelona, Spain. Atmos. Environ. 40, 2180-2193. https://dio.org/10.1016/j.atmosenv.2005.12.001
58. Walker, S., 1999. Uncontrolled Fires in Coal and Coal Wastes, Coal Research.
59. Wang, F.Y., 2016. Study on the morphologic transformation mechanism of mercury in industrial flue gas, Tsinghua university. Tsinghua university, Beijing. (in Chinese)
60. Wang, Z., Dong, S.P., Liang, H.D., Chen, Y., Zhan, Q., 2018. Study on environmental individual particles in Wuda-Wusitai Industrial Park, Inner Mongolia. China Environmental Science 38:478-489. DOI: 10.19674/j.cnki.issn1000-6923.2018.0055
61. Wang, Z., Chen, Z., Duan, N., Zhang, X., 2007. Gaseous elemental mercury concentration in atmosphere at urban and remote sites in China. Journal of Environmental Sciences, 19(2): 176–180. doi:10.1016/s1001-0742(07)60028-x
62. Weiss-Penzias, P., Amos, H., Selin, N., Gustin, M., Jaffe, D., Obrist, D., et al., 2015. Use of a global model to understand speciated atmospheric mercury observations at five high-elevation sites. Atmos. Chem. Phys. 15, 1161-1173.
63. Windham-Myers, L., Marvin-DiPasquale, M., Stricker, C.A., Agee, J.L., Kieu, L.H., Kakouros, E., 2013. Mercury cycling in agricultural and managed wetlands of California, USA:Experimental evidence of vegetation-driven changes in sediment biogeochemistry and methylmercury production. Sci. Total Environ. 484, 300-307. https://dio.org/10.1016/j.scitotenv.2013.05.028
64. Xiu, G.L., Shi, S.Y., Zhang, D.N., 2003. Preliminary study on characteristics of particulate mercury in fine particles in ambient air. Shanghai environmental science 22(5):310-316. (in Chinese)
65. Yang, L.Y., Zhang, W., Ren, M.Y., Cao, F.F., Chen, F.F., Zhang, Y.T., Shang, L.H., 2020. Mercury distribution in a typical shallow lake in northern China and its reemission from sediment Ecotoxicology and Environmental Safety 192. https://dio.org/10.1016/j.ecoenv.2020.110316
66. Zhang, L., Lyman, S., Mao, H., Lin, C., Gay, D., Wang, S., et al., 2017. A synthesis of research needs for improving the understanding of atmospheric mercury cycling. Atmos. Chem. Phys., 17, 9133-9144. DOI: 10.5194/acp-17-9133-2017

67. Zhang, R., Jing, J., Tao, J., Hsu, S.-C., Wang, G., Cao, J., Lee, C. S. L., Zhu, L., Chen, Z., Zhao, Y., Shen, Z., 2013. Chemical characterization and source apportionment of TSP in Beijing: seasonal perspective. Atmos. Chem. Phys., 13(14):7053-7074.

68. Zhang, X.M., Kroonenberg, S.B., de Boer, C.B., 2004. Dating of coal fires in Xinjiang, north-west China. Terra Nova 16, 68-74. https://dio.org/10.1111/j.1365-3121.2004.00532.x

Tables

Table 1

Correlation coefficient (r) of PHg content and water-soluble ion content in $PM_{2.5}$

	PM	F^-	Cl^-	NO_2^-	NO_3^-	SO_4^{2-}	Na^+	NH_4^+	K^+	Mg^{2+}	Ca^{2+}
PM	1	-0.012	0.854**	0.138	0.745**	0.534	0.758**	0.032	.378	0.720*	0.753**
F^-		1	-0.071	0.404	-0.289	0.351	-0.047	0.840**	0.467	-0.129	-0.123
Cl^-			1	0.120	0.598	0.218	0.633*	-0.093	0.146	0.835**	0.799**
NO_2^-				1	-0.367	-0.046	-0.274	0.436	0.287	-0.108	-0.070
NO_3^-					1	0.589	0.882**	-0.281	0.112	0.658*	0.683*
SO_4^{2-}						1	0.690*	0.502	0.516	0.271	0.208
Na^+							1	-0.088	0.000	0.757**	0.714*
NH_4^+								1	0.685*	-0.161	-0.266
K^+									1	-0.158	-0.148
Mg^{2+}										1	0.937**
Ca^{2+}											1

** significant correlation at 0.01 level; * significant correlation at 0.05 level.

Table 2
Correlation coefficient (r) of PHg content and water-soluble ion content in TSP

	PM	F^-	Cl^-	NO_2^-	NO_3^-	SO_4^{2-}	Na^+	NH_4^+	K^+	Mg^{2+}	Ca^{2+}
PM	1	-0.711**	0.020	0.304	0.644*	0.479	0.162	-0.089	0.336	0.224	0.308
F^-		1	0.002	-0.288	-0.528	-0.659*	-0.301	0.674*	-0.459	-0.573	-0.414
Cl^-			1	-0.299	0.225	-0.069	0.890**	.226	0.519	0.093	0.211
NO_2^-				1	-0.052	0.323	-0.079	-0.173	0.153	0.237	0.243
NO_3^-					1	0.439	0.394	-0.178	0.679*	0.521	0.521
SO_4^{2-}						1	0.040	-0.724**	0.544	0.849**	0.762**
Na^+							1	0.013	0.624*	0.278	0.317
NH_4^+								1	-0.291	0-.767**	-0.399
K^+									1	0.695*	.805**
Mg^{2+}										1	0.841**
Ca^{2+}											1
** significant correlation at 0.01 level; * significant correlation at 0.05 level.											

Table 3
Thermal decomposition temperatures of mercury compounds in argon

Mercury compound	Center peak (°C)	Starting-ending range (°C)	References
$HgCl_2$	212 ± 15	130–390	(Lv, 2017; Wang, 2016)
HgS(red)	310 ± 15	240–350	(Lopez-Anton et al., 2011; Meng and Wang, 2012)
HgO	340 ± 15	310–380	(Liu et al., 2013; Wang, 2016)
$Hg(NO_3)_2{\cdot}H_2O$	373 ± 15	310–400	(Lv, 2017)
$HgSO_4$	540 ± 15	500–600	(Lopez-Anton et al., 2011; Lv, 2017)

Figures

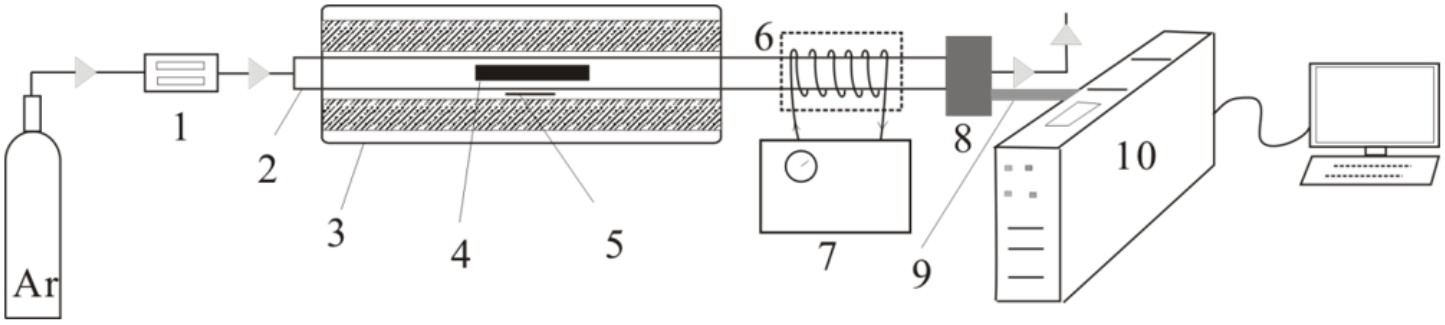

Figure 1

Schematic diagram of the temperature-programmed desorption experimental system (1 flow meter; 2 quartz tube; 3 tube pyrolysis furnace; 4 coal sample; 5 temperature controller; 6 sample cooling zone; 7 circulating water cooler; 8 Pyro-915+ cracker (800 °C); 9 optical path channel; 10 RA-915 mercury analyzer. The circulating water cooler was not used in the TPD experiment.)

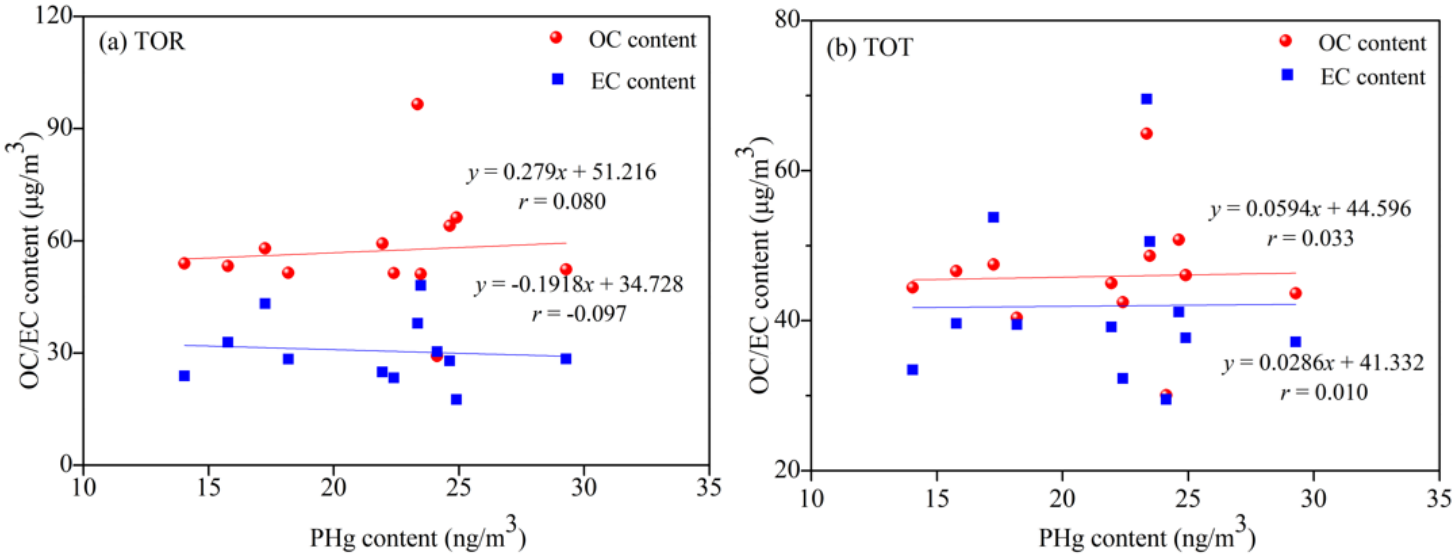

Figure 2

Correlation between PHg and OC/EC content in TSP

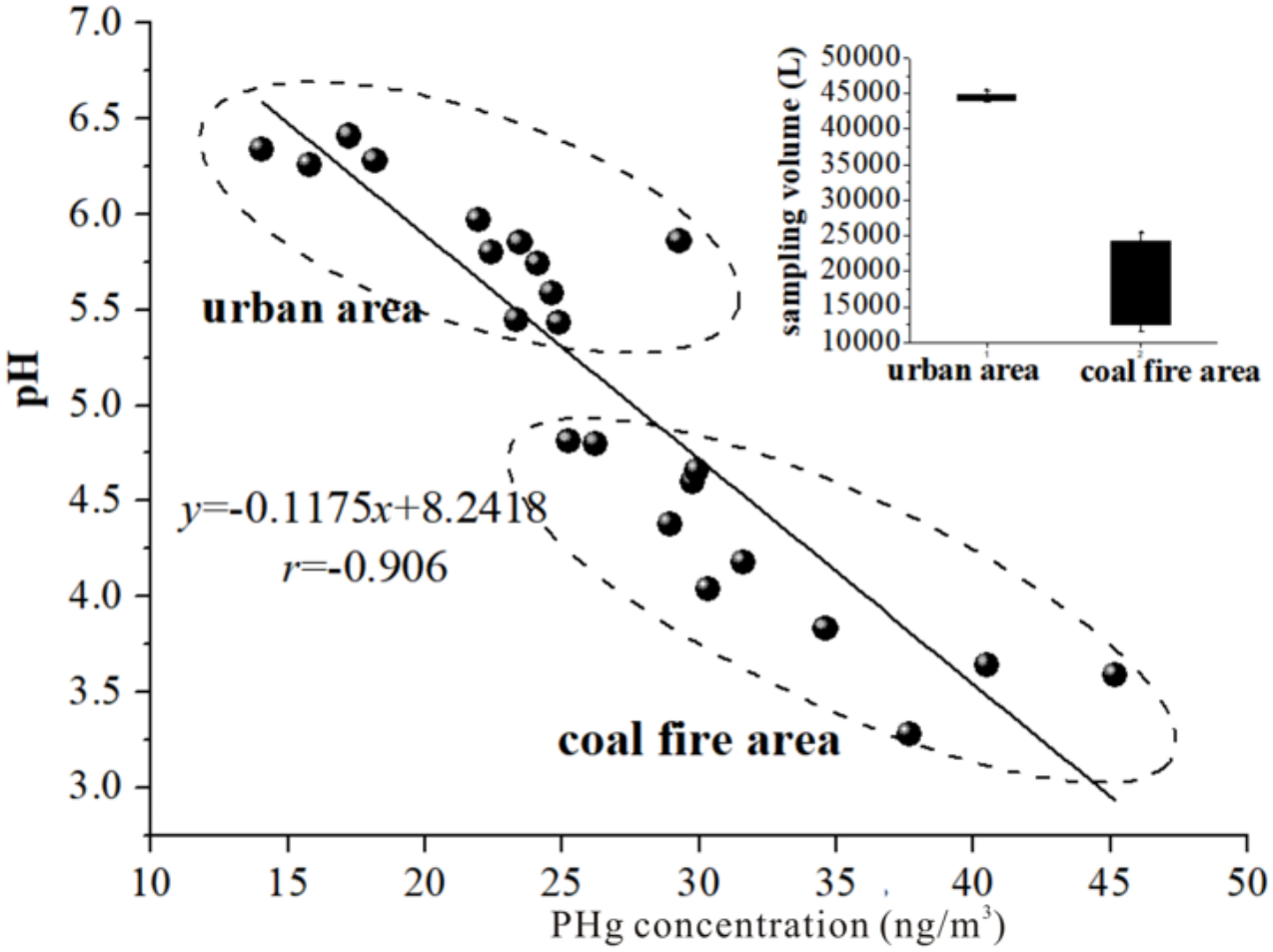

Figure 3

Correlation between PHg content and pH

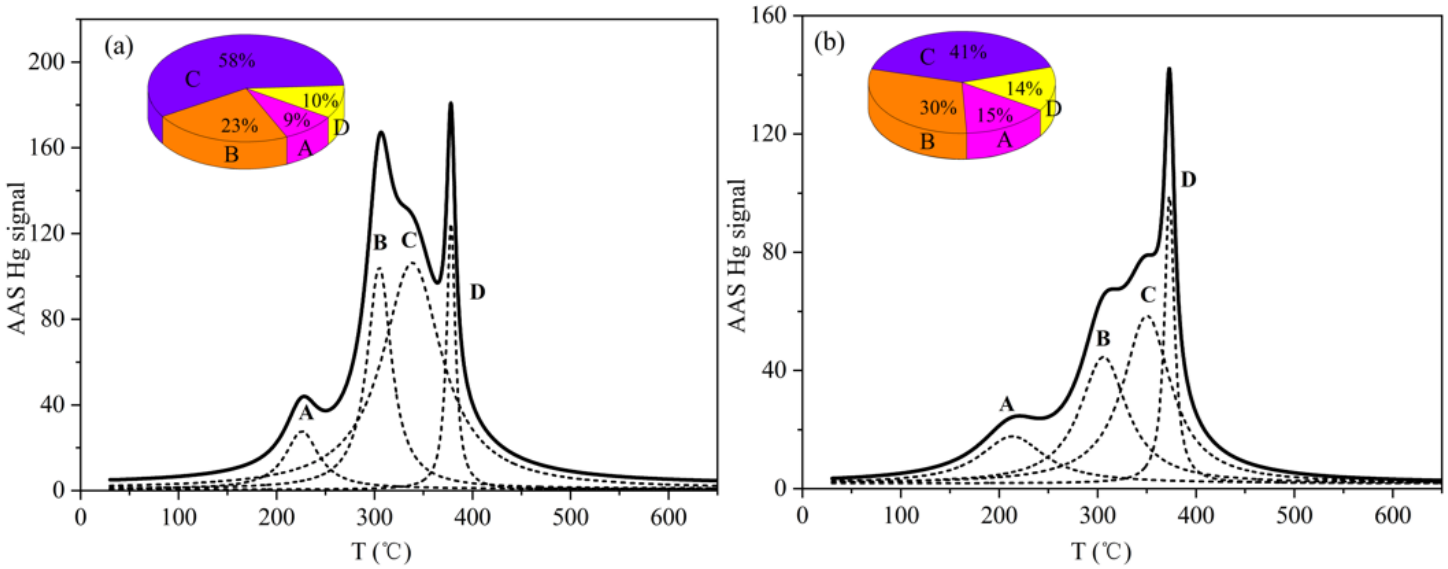

Figure 4

Thermal decomposition curves of Hg in TSP samples: (a) coalfield area; (b) urban area.